IOP Publishing Journal of Micromechanics and Microengineering

J. Micromech. Microeng. **19** (2009) 025011 (8pp) doi:10.1088/0960-1317/19/2/025011

Fully compliant double tensural tristable micromechanisms (DTTM)

Guimin Chen[1,3], Daniel L Wilcox[2] and Larry L Howell[3]

[1] School of Mechatronics, Xidian University, Xi'an, Shaanxi 710071, People's Republic of China
[2] Sandia National Laboratories, Albuquerque, NM 87185, USA
[3] Mechanical Engineering Department, Brigham Young University, Provo, UT 84602, USA

Received 5 September 2008, in final form 27 October 2008
Published 14 January 2009
Online at stacks.iop.org/JMM/19/025011

Abstract
Numerous possible micromechanism applications (e.g. three-way switches, mechanical memory and multiplex optical switches) could benefit from a device with three stable equilibrium positions. In this paper, we present a new class of tristable mechanisms called double tensural tristable mechanisms (DTTMs) which are fully compliant (i.e. they are monolithic and get their motion from the deflection of elastic components) and can be fabricated at the micro scale. A pseudo-rigid-body model (PRBM) for the DTTM has been developed. DTTMs were fabricated in polysilicon using the SUMMiT V process and tested for tristability and force–deflection characteristics. The results successfully demonstrate tristable behavior and show that the PRBM can be used to identify tristable configurations and predict their performance.

(Some figures in this article are in colour only in the electronic version)

1. Introduction

A multistable mechanism has two or more positions within its range of motion in which the device is stable. In these positions, the mechanism can maintain stability without power input and with high repeatability. A compliant mechanism, which achieves at least some of its mobility from the deflection of the flexible segments rather than from movable joints only, offers a solution for multistable mechanisms because the flexible segments store potential energy as they deflect [1].

Much study and research has been devoted to bistable mechanisms at both macro [2–5] and micro levels [5–13]. However, few mechanism examples have been presented that exhibit three or more mechanically stable positions. Oberhammer *et al* [14] presented a tristable latching structure for single-pole-double-throw micro-switches. Pendleton and Jensen [15] presented a tristable compliant mechanism based on a symmetric four-bar Grashof mechanism. Han *et al* [16] demonstrated a quadstable monolithic mechanism (provides four stable states), which is realized by nesting two bistable structures in X and Y directions, respectively. Foulds *et al* [9] proposed a mechanical bistable switch based on a locking mechanism, which can be extended to multi-stable switches. Ohsaki and Nishiwaki [17] presented an approach to generating multi-stable compliant mechanisms using pin-jointed bar elements. In their approach, the unstable equilibrium state is limited by locking the actuator and the device behaves as if it is in a stable equilibrium position. Oh and Kota [18] present a synthesis method of multi-stable compliant mechanisms by connecting multiple bistable mechanisms of different load thresholds in series. King *et al* [19, 20] proposed an optimization-based synthesis method for multi-stable mechanisms spanning various energy domains.

2. Tristable mechanisms

Figure 1 shows a 'ball-on-the-hill' analogy for a tristable mechanism. For the series of hills and valleys shown in the figure, a ball would be stable if placed in any of the three valleys because the ball would return to its position after a small disturbance. In a tristable mechanism, three equilibrium positions are stable, maintaining state despite small disturbances and requiring no power input to maintain the state. Numerous possible micromechanism applications could benefit from a device with three stable equilibrium positions, including three-way switches [14], mechanical memory and multiplex optical switches.

In this paper, we present a new class of tristable mechanisms called double tensural tristable mechanisms (DTTMs) which are fully compliant and can be fabricated

 © 2009 IOP Publishing Ltd Printed in the UK

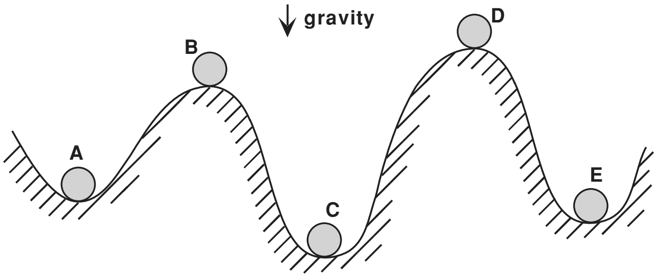

Figure 1. The ball-on-a-hill analogy for a mechanically tristable mechanism.

at the MEMS scale. Because compliant mechanisms use deflection of flexible members to obtain their motion, the friction associated with articulating joints is eliminated. It is also possible to use compliant mechanisms to achieve sophisticated motions with a single layer of material [1]. The fully compliant nature of the device provides advantages in fabrication and friction compared to other possible tristable devices. Figure 2 shows a scanning electron micrograph of a DTTM. The pseudo-rigid-body model is also developed, which can be used to design DTTMs and ensure their tristability. A schematic of the DTTM in its three stable equilibrium positions is shown in figure 3.

3. DTTM and its pseudo-rigid-body model

The secrets of the tristable mechanism's operation are found in the fundamentals of certain bistable micromechanisms [5, 13] that use flexible elements experiencing combined tension and bending. As reported in [13], some double-tensural bistable mechanism (DTBM) configurations exhibit soft spring-like behavior when deflected past the second equilibrium position (post-bistable behavior). Further study reveals that some DTBM configurations also exhibit soft spring-like behavior when pulled in the opposite direction from the fabricated position. The explanation of such behavior is that the tensural pivots become conventional flexural pivots which undergo combined compression and bending when DTBMs are pulled

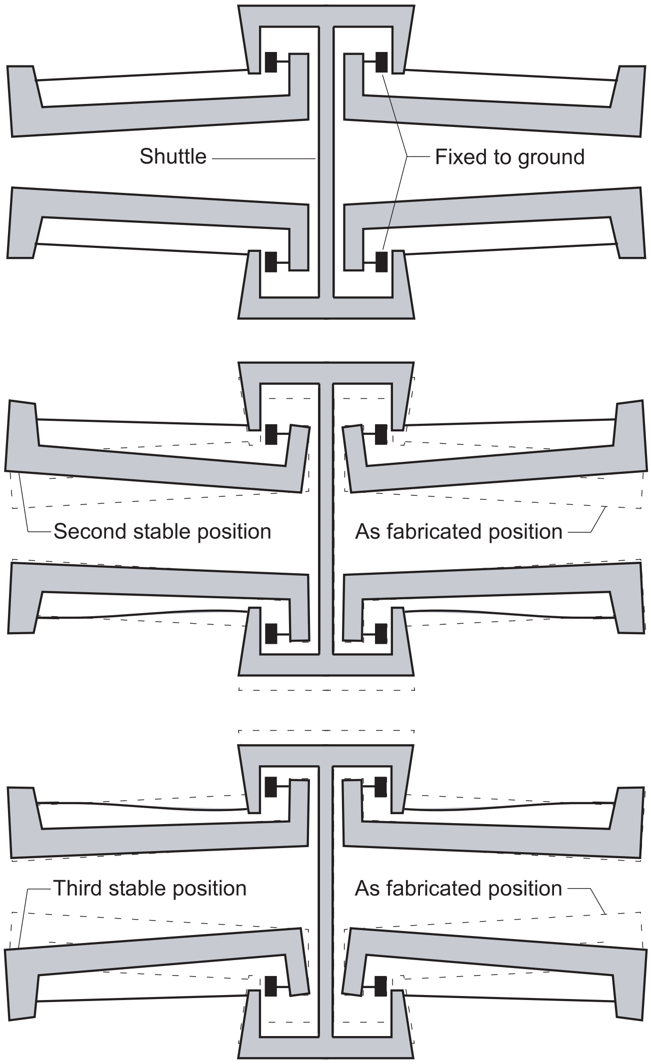

Figure 3. The DTTM illustrated in its three stable equilibrium positions, including its as-fabricated position (top), second stable position (middle) and third stable position (bottom).

in the opposite direction. This is key to DTTM behavior because one DTBM coupled with a DTBM inversion has the

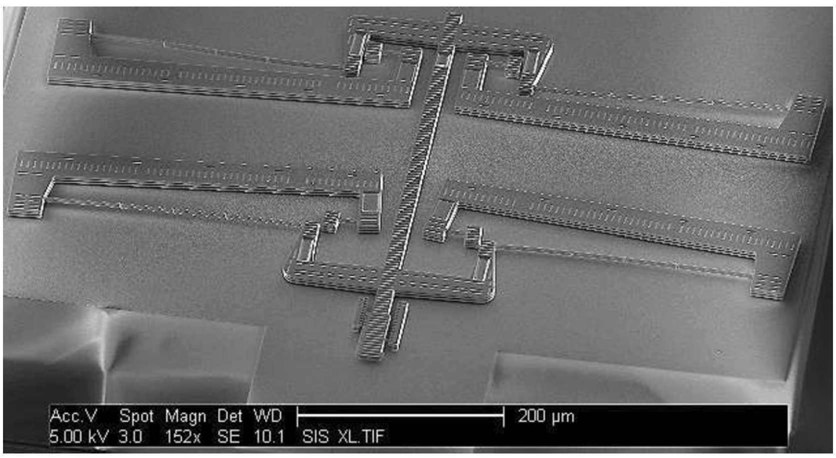

Figure 2. Scanning electron micrograph of a fully compliant tristable mechanism. Position measurements are made using the attached vernier.

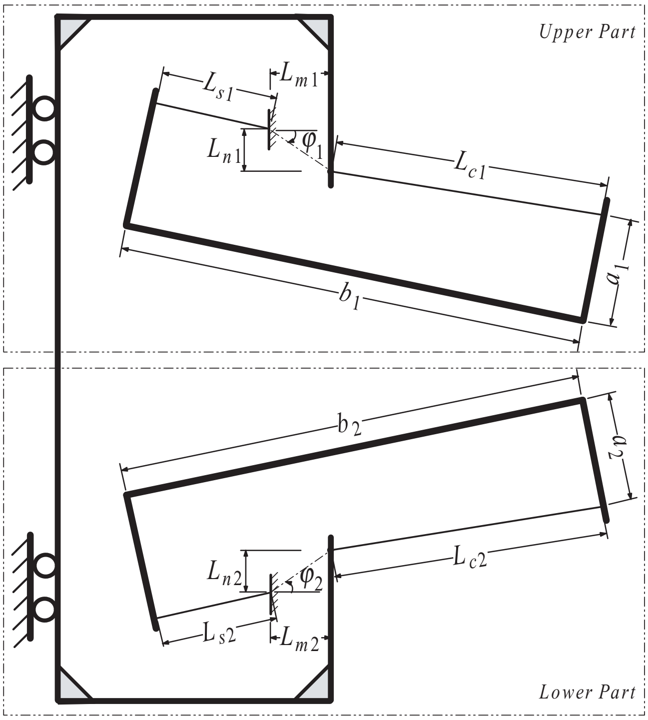

Figure 4. Half model of the double tensural tristable mechanism (DTTM). The DTTM is symmetric about the rollers, which represent the shuttle.

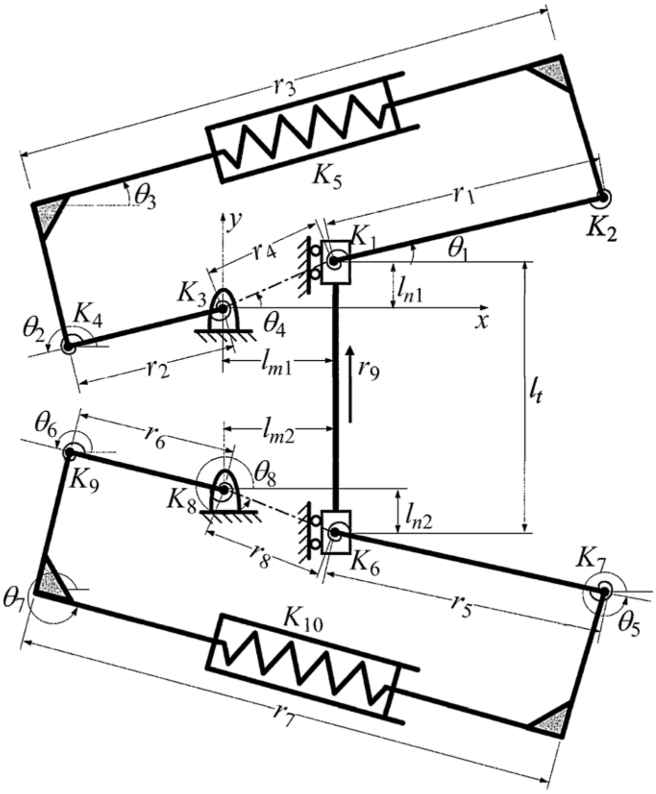

Figure 5. The pseudo-rigid-body model of half a double tensural tristable mechanism. The shuttle is represented with an abstract, but kinematically accurate, rigid bar connecting the upper and lower parts. Because the bar is rigid, it can be shown connecting the two parts directly regardless of where the components lie in space.

potential for exhibiting tristable behavior. Figure 4 shows the layout and the design parameters of the half model. In addition to the parameters shown in figure 4, h_{c1}, h_{s1}, h_{c2} and h_{s2} refer to the out-of-plane thicknesses of the flexible segments with lengths L_{c1}, L_{s1}, L_{c2} and L_{s2}. Likewise, w_{c1}, w_{s1}, w_{c2} and w_{s2} refer to the in-plane thicknesses of these same segments. The out-of-plane thicknesses and widths of the frames (with features labeled a_i and b_i in figure 4) are h_{f1}, h_{f2}, w_{f1} and w_{f2}. When pulling up, the upper part of the model behaves as a soft spring while the lower part acts like a bistable mechanism. However, when pulling down, the roles are reversed and the upper part of the model behaves as a bistable mechanism while the lower part as a soft spring.

Figure 5 shows a pseudo-rigid-body model [1] of the DTTM. The PRBM treats the tensural pivots as fixed-guided segments, which results in three degree-of-freedom mechanisms for both the upper and lower parts. Although two of the degrees of freedom for each part are unconstrained, the principle of virtual work can be used to determine the mechanism position because the device will tend toward the position of minimum potential energy.

To facilitate the device description and design, it is assumed that the upper and lower parts are of the same dimensions, i.e., $L_{c1} = L_{c2} = L_c, L_{s1} = L_{s2} = L_s, h_{c1} = h_{c2} = h_c, h_{s1} = h_{s2} = h_s, w_{c1} = w_{c2} = w_c, w_{s1} = w_{s2} = w_s, L_{c1} = L_{c1} = L_c, L_{m1} = L_{m2} = L_m, L_{n1} = L_{n2} = L_n, a_1 = a_2 = a$ and $b_1 = b_2 = b$. This symmetry results in symmetry of the stable equilibrium positions. Selecting nonsymmetric values can result in nonsymmetric placement of equilibrium positions. The force characteristics would also be affected; each direction could be tailored to specific force–deflection characteristics, which may benefit some applications. The link lengths, and spring constants for the model can be calculated as follows:

$$r_1 = r_5 = \gamma L_c \tag{1}$$

$$r_2 = r_6 = \gamma L_s \tag{2}$$

$$\varphi_1 = \varphi_2 = \arctan \frac{L_n}{L_m} \tag{3}$$

$$l_{m1} = l_{m2} = L_m + \frac{1-\gamma}{2} L_c \cos\theta_{1o} - \frac{1-\gamma}{2} L_s \cos\theta_{2o} \tag{4}$$

$$l_{n1} = l_{n2} = L_n + \frac{1-\gamma}{2} L_c \sin\theta_{1o} - \frac{1-\gamma}{2} L_s \sin\theta_{2o} \tag{5}$$

$$\theta_{4o} = 2\pi - \theta_{8o} = \arctan \frac{l_{n1}}{l_{m1}} \tag{6}$$

$$\theta_{3o} = 2\pi - \theta_{7o} = \arctan \frac{r_1 \sin\theta_{1o} + l_{n1} - r_2 \sin\theta_{2o}}{r_1 \cos\theta_{1o} + l_{m1} - r_2 \cos\theta_{2o}} \tag{7}$$

$$r_{3o} = r_{7o} = \frac{r_1 \cos\theta_{1o} + l_{m1} - r_2 \cos\theta_{2o}}{\cos\theta_{3o}} \tag{8}$$

$$K_1 = K_2 = K_6 = K_7 = 2\gamma K_\Theta \frac{EI_c}{L_c} \tag{9}$$

$$K_3 = K_4 = K_8 = K_9 = 2\gamma K_\Theta \frac{EI_s}{L_s}, \tag{10}$$

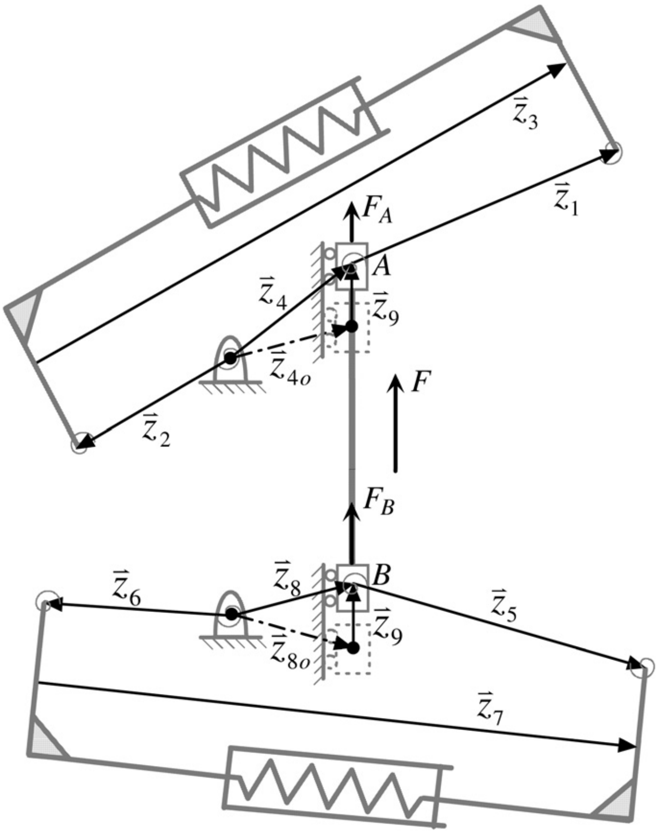

Figure 6. Vector loop diagram superposed on the PRBM.

where γ is the characteristic radius factor, K_Θ is the stiffness coefficient for the torsional springs, E is the Young's modulus of the material, $I_c = h_c w_c^3/12$ and $I_s = h_s w_s^3/12$. In this paper, $\gamma = 0.65$ and $K_\Theta = 1.45$ [22] were used to calculate the force–deflection behavior of the PRBM.

K_5 and K_{10} are the equivalent spring constants of the frames together with the tensural pivots for the upper and lower parts, respectively. These spring constants include the effects due to axial compression of the frame, axial elongation of the tensural pivots, and bending of the frame. The spring constant is found by combining the equivalent springs of these individual components as springs in series. Assuming all frame components have the same cross-section,

$$K_5 = K_{10} = \frac{1}{\frac{a^2 b}{EI} + \frac{2a^3}{3EI} + \frac{b}{EA} + \frac{L_c}{EA_c} + \frac{L_s}{EA_s}}, \tag{11}$$

where $A_c = h_c w_c$, $A_s = h_s w_s$, $I = h_f w_f^3/12$ and $A = h_f w_f$. Although these springs are very stiff and result in small deflections, these deflections are still critical for the behavior of the mechanism [12, 22].

3.1. Principle of virtual work

A vector loop [21] for the PRBM of the DTTM upper part above is written as

$$\vec{z}_2 + \vec{z}_3 = \vec{z}_{4o} + \vec{z}_9 + \vec{z}_1 \tag{12}$$

and a vector loop for the lower part is written as

$$\vec{z}_6 + \vec{z}_7 = \vec{z}_{8o} + \vec{z}_9 + \vec{z}_5 \tag{13}$$

where the vectors are as shown in figure 6. These vectors correspond to $r_1, r_2, ..., r_9, l_{m1}, l_{n1}, l_{m2}$ and l_{n2} as shown in figure 5. These vectors may be represented by the Cartesian vectors:

$$\vec{X}_A \Rightarrow r_2 \cos\theta_2 + r_3 \cos\theta_3 = l_{m1} + r_1 \cos\theta_1 \tag{14}$$

$$\vec{Y}_A \Rightarrow r_2 \sin\theta_2 + r_3 \sin\theta_3 = l_{n1} + r_9 + r_1 \sin\theta_1 \tag{15}$$

$$\vec{X}_B \Rightarrow r_6 \cos\theta_6 + r_7 \cos\theta_7 = l_{m2} + r_5 \cos\theta_5 \tag{16}$$

$$\vec{Y}_B \Rightarrow r_6 \sin\theta_6 + r_7 \sin\theta_7 = -l_{n2} + r_9 + r_5 \sin\theta_5, \tag{17}$$

where the subscript 'A' refers to the upper part and the subscript 'B' refers to the lower part.

The applied force can be expressed in a vector form as

$$\vec{F} = F\hat{j} = F_A\hat{j} + F_B\hat{j}, \tag{18}$$

where F_A is the force component needed to actuate the upper part, and F_B is the force component needed to actuate the lower part.

The force placement (with respect to the origin) is expressed in a vector form as

$$\vec{z}_A = l_{m1}\hat{i} + (l_{n1} + r_9)\hat{j} \tag{19}$$

$$\vec{z}_B = l_{m2}\hat{i} + (-l_t - l_{n2} + r_9)\hat{j} \tag{20}$$

where l_t is the length of the shuttle.

Generalized coordinates are selected for the upper (q_i) and lower (p_i) parts as

$$\begin{array}{lll} q_1 = \theta_1, & q_2 = \theta_2, & q_3 = \theta_3, \\ p_1 = \theta_5, & p_2 = \theta_6, & p_3 = \theta_7. \end{array} \tag{21}$$

Tables 1 and 2 list the virtual displacements found by differentiating equations (19) and (20) with respect to the generalized coordinates. The resulting kinematic coefficients are based on the partial derivatives (with respect to the generalized coordinates) of the vector loop equations for the mechanism:

$$\begin{aligned}
&\frac{\partial \vec{X}_A}{\partial q} \Rightarrow -r_2 \sin\theta_2 \frac{\partial \theta_2}{\partial q} + \cos\theta_3 \frac{\partial r_3}{\partial q} - r_3 \sin\theta_3 \frac{\partial \theta_3}{\partial q} \\
&\quad = -r_1 \sin\theta_1 \frac{\partial \theta_1}{\partial q} \\
&\frac{\partial \vec{Y}_A}{\partial q} \Rightarrow r_2 \cos\theta_2 \frac{\partial \theta_2}{\partial q} + \sin\theta_3 \frac{\partial r_3}{\partial q} + r_3 \cos\theta_3 \frac{\partial \theta_3}{\partial q} \\
&\quad = \frac{\partial r_9}{\partial q} + r_1 \cos\theta_1 \frac{\partial \theta_1}{\partial q} \\
&\frac{\partial \vec{X}_B}{\partial p} \Rightarrow -r_6 \sin\theta_6 \frac{\partial \theta_6}{\partial p} + \cos\theta_7 \frac{\partial r_7}{\partial p} - r_7 \sin\theta_7 \frac{\partial \theta_7}{\partial p} \\
&\quad = -r_5 \sin\theta_5 \frac{\partial \theta_5}{\partial p} \\
&\frac{\partial \vec{Y}_B}{\partial p} \Rightarrow r_6 \cos\theta_6 \frac{\partial \theta_6}{\partial p} + \sin\theta_7 \frac{\partial r_7}{\partial p} + r_7 \cos\theta_7 \frac{\partial \theta_7}{\partial p} \\
&\quad = \frac{\partial r_9}{\partial p} + r_5 \cos\theta_5 \frac{\partial \theta_5}{\partial p}.
\end{aligned} \tag{22}$$

The kinematic coefficients are listed in table 3.

The virtual work, δW, due to the input force is the dot product of the force vector and the virtual displacement

Table 1. Partial derivatives of coordinates.

Coordinate	$\delta\Theta_1 = \sum \frac{\partial\phi\delta q_1}{\partial q_1}$	$\delta\Theta_2 = \sum \frac{\partial\phi\delta q_2}{\partial q_2}$	$\delta\Theta_3 = \sum \frac{\partial\phi\delta q_3}{\partial q_3}$
$\vec{z}_A = l_{m1}\hat{i} + (l_{n1} + r_9)\hat{j}$	$\frac{\partial\vec{z}_A}{\partial\theta_1}\delta\theta_1 = \frac{dr_9}{d\theta_1}\delta\theta_1$	$\frac{\partial\vec{z}_A}{\partial\theta_2}\delta\theta_2 = \frac{dr_9}{d\theta_2}\delta\theta_2$	$\frac{\partial\vec{z}_A}{\partial\theta_3}\delta\theta_3 = \frac{dr_9}{d\theta_3}\delta\theta_3$
$\phi_1 = (\theta_1 - \theta_{1o})$	$\frac{\partial\phi_1}{\partial\theta_1}\delta\theta_1 = \delta\theta_1$	$\frac{\partial\phi_1}{\partial\theta_2}\delta\theta_2 = 0$	$\frac{\partial\phi_1}{\partial\theta_3}\delta\theta_3 = 0$
$\phi_2 = [(\theta_1 - \theta_{1o}) - (\theta_3 - \theta_{3o})]$	$\frac{\partial\phi_2}{\partial\theta_1}\delta\theta_1 = \delta\theta_1$	$\frac{\partial\phi_2}{\partial\theta_2}\delta\theta_2 = 0$	$\frac{\partial\phi_2}{\partial\theta_3}\delta\theta_3 = -\delta\theta_3$
$\phi_3 = (\theta_2 - \theta_{2o})$	$\frac{\partial\phi_3}{\partial\theta_1}\delta\theta_1 = 0$	$\frac{\partial\phi_3}{\partial\theta_2}\delta\theta_2 = \delta\theta_2$	$\frac{\partial\phi_3}{\partial\theta_3}\delta\theta_3 = 0$
$\phi_4 = [(\theta_2 - \theta_{2o}) - (\theta_3 - \theta_{3o})]$	$\frac{\partial\phi_4}{\partial\theta_1}\delta\theta_1 = 0$	$\frac{\partial\phi_4}{\partial\theta_2}\delta\theta_2 = \delta\theta_2$	$\frac{\partial\phi_4}{\partial\theta_3}\delta\theta_3 = -\delta\theta_3$
$R_A = (r_3 - r_{3o})$	$\frac{\partial R_A}{\partial\theta_1}\delta\theta_1 = \frac{dr_3}{d\theta_1}\delta\theta_1$	$\frac{\partial R_A}{\partial\theta_2}\delta\theta_2 = \frac{dr_3}{d\theta_2}\delta\theta_2$	$\frac{\partial R_A}{\partial\theta_3}\delta\theta_3 = \frac{dr_3}{d\theta_3}\delta\theta_3$

Table 2. Partial derivatives of coordinates.

Coordinate	$\delta\Theta_5 = \sum \frac{\partial\phi\delta p_1}{\partial p_1}$	$\delta\Theta_6 = \sum \frac{\partial\phi\delta p_2}{\partial p_2}$	$\delta\Theta_7 = \sum \frac{\partial\phi\delta p_3}{\partial p_3}$
$\vec{z}_B = l_{m2}\hat{i} + (-l_t - l_{n2} + r_9)\hat{j}$	$\frac{\partial\vec{z}_B}{\partial\theta_5}\delta\theta_5 = \frac{dr_9}{d\theta_5}\delta\theta_5$	$\frac{\partial\vec{z}_B}{\partial\theta_6}\delta\theta_6 = \frac{dr_9}{d\theta_6}\delta\theta_6$	$\frac{\partial\vec{z}_B}{\partial\theta_7}\delta\theta_7 = \frac{dr_9}{d\theta_7}\delta\theta_7$
$\phi_5 = (\theta_5 - \theta_{5o})$	$\frac{\partial\phi_5}{\partial\theta_5}\delta\theta_5 = \delta\theta_5$	$\frac{\partial\phi_5}{\partial\theta_6}\delta\theta_6 = 0$	$\frac{\partial\phi_5}{\partial\theta_7}\delta\theta_7 = 0$
$\phi_6 = [(\theta_5 - \theta_{5o}) - (\theta_7 - \theta_{7o})]$	$\frac{\partial\phi_6}{\partial\theta_5}\delta\theta_5 = \delta\theta_5$	$\frac{\partial\phi_6}{\partial\theta_6}\delta\theta_6 = 0$	$\frac{\partial\phi_6}{\partial\theta_7}\delta\theta_7 = -\delta\theta_7$
$\phi_7 = (\theta_6 - \theta_{6o})$	$\frac{\partial\phi_7}{\partial\theta_5}\delta\theta_5 = 0$	$\frac{\partial\phi_7}{\partial\theta_6}\delta\theta_6 = \delta\theta_6$	$\frac{\partial\phi_7}{\partial\theta_7}\delta\theta_7 = 0$
$\phi_8 = [(\theta_6 - \theta_{6o}) - (\theta_7 - \theta_{7o})]$	$\frac{\partial\phi_8}{\partial\theta_5}\delta\theta_5 = 0$	$\frac{\partial\phi_8}{\partial\theta_6}\delta\theta_6 = \delta\theta_6$	$\frac{\partial\phi_8}{\partial\theta_7}\delta\theta_7 = -\delta\theta_7$
$R_B = (r_7 - r_{7o})$	$\frac{\partial R_B}{\partial\theta_5}\delta\theta_5 = \frac{dr_7}{d\theta_5}\delta\theta_5$	$\frac{\partial R_B}{\partial\theta_6}\delta\theta_6 = \frac{dr_7}{d\theta_6}\delta\theta_6$	$\frac{\partial R_B}{\partial\theta_7}\delta\theta_7 = \frac{dr_7}{d\theta_7}\delta\theta_7$

Table 3. Kinematic coefficients.

$\frac{\partial r_3}{\partial q}$	$\frac{\partial r_9}{\partial q}$	$\frac{\partial r_7}{\partial p}$	$\frac{\partial r_9}{\partial p}$
$\frac{dr_3}{d\theta_1} = -\frac{r_1\sin\theta_1}{\cos\theta_3}$	$\frac{dr_9}{d\theta_1} = -\frac{r_1\cos(\theta_1-\theta_3)}{\cos\theta_3}$	$\frac{dr_7}{d\theta_5} = -\frac{r_5\sin\theta_5}{\cos\theta_7}$	$\frac{dr_9}{d\theta_5} = -\frac{r_5\cos(\theta_5-\theta_7)}{\cos\theta_7}$
$\frac{dr_3}{d\theta_2} = \frac{r_2\sin\theta_2}{\cos\theta_3}$	$\frac{dr_9}{d\theta_2} = \frac{r_2\cos(\theta_2-\theta_3)}{\cos\theta_3}$	$\frac{dr_7}{d\theta_6} = \frac{r_6\sin\theta_6}{\cos\theta_7}$	$\frac{dr_9}{d\theta_6} = \frac{r_6\cos(\theta_6-\theta_7)}{\cos\theta_7}$
$\frac{dr_3}{d\theta_3} = \frac{r_3\sin\theta_3}{\cos\theta_3}$	$\frac{dr_9}{d\theta_3} = \frac{r_3}{\cos\theta_3}$	$\frac{dr_7}{d\theta_7} = \frac{r_7\sin\theta_7}{\cos\theta_7}$	$\frac{dr_9}{d\theta_7} = \frac{r_7}{\cos\theta_7}$

($\delta W = F\cdot dz$). If the moment at spring i is T_i (where $T_i = -K_i\phi_i$, with ϕ_i the angular displacement of the torsional spring), then the virtual work, δW, due to the moments is $\delta W = \sum T_i \cdot d\phi_i$. The potential energy in K_5 and K_{10} can be modeled as

$$\delta W_{As} = \sum \frac{\partial P_{As}}{\partial q}(-\delta q) = F_{As}\left(\frac{dr_3}{d\theta_1}\delta\theta_1 + \frac{dr_3}{d\theta_2}\delta\theta_2 + \frac{dr_3}{d\theta_3}\delta\theta_3\right) \tag{23}$$

$$\delta W_{Bs} = \sum \frac{\partial P_{Bs}}{\partial p}(-\delta p) = F_{Bs}\left(\frac{dr_7}{d\theta_5}\delta\theta_5 + \frac{dr_7}{d\theta_6}\delta\theta_6 + \frac{dr_7}{d\theta_7}\delta\theta_7\right). \tag{24}$$

Applying the principle of virtual work by summing the virtual work due to the input force, applied moments, and frame spring and setting equal to zero, results in

$$\delta W_A = \vec{F}_A \cdot d\vec{z}_A + T_1\, d\phi_1 + T_2\, d\phi_2 + T_3\, d\phi_3 + T_4\, d\phi_4 + F_{As}\, dR_A = 0 \tag{25}$$

$$\delta W_B = \vec{F}_B \cdot d\vec{z}_B + T_5\, d\phi_5 + T_6\, d\phi_6 + T_7\, d\phi_7 + T_8\, d\phi_8 + F_{Bs}\, dR_B = 0. \tag{26}$$

Combining the partial derivatives in tables 1 and 2 with the kinematic coefficients in table 3 and grouping the resulting equations by generalized coordinates, results in the following equations which define the motion of the system:

$$\begin{cases} F_A\frac{dr_9}{d\theta_1} + T_1 + T_2 + F_{As}\frac{dr_3}{d\theta_1} = 0 \\ F_A\frac{dr_9}{d\theta_2} + T_3 + T_4 + F_{As}\frac{dr_3}{d\theta_2} = 0 \\ F_A\frac{dr_9}{d\theta_3} - T_2 - T_4 + F_{As}\frac{dr_3}{d\theta_3} = 0 \end{cases} \tag{27}$$

$$\begin{cases} F_B\frac{dr_9}{d\theta_5} + T_5 + T_6 + F_{Bs}\frac{dr_7}{d\theta_5} = 0 \\ F_B\frac{dr_9}{d\theta_6} + T_7 + T_8 + F_{Bs}\frac{dr_7}{d\theta_6} = 0 \\ F_B\frac{dr_9}{d\theta_7} - T_6 - T_8 + F_{Bs}\frac{dr_7}{d\theta_7} = 0. \end{cases} \tag{28}$$

Considering the shuttle displacement, r_9, to be a known input (with a positive value for r_9 representing an upward displacement), the following relationships result:

$$\theta_4 = \arctan\left(\frac{l_{n1} + r_9}{l_{m1}}\right) \tag{29}$$

$$\theta_8 = 2\pi - \arctan\left(\frac{l_{n2} - r_9}{l_{m2}}\right) \tag{30}$$

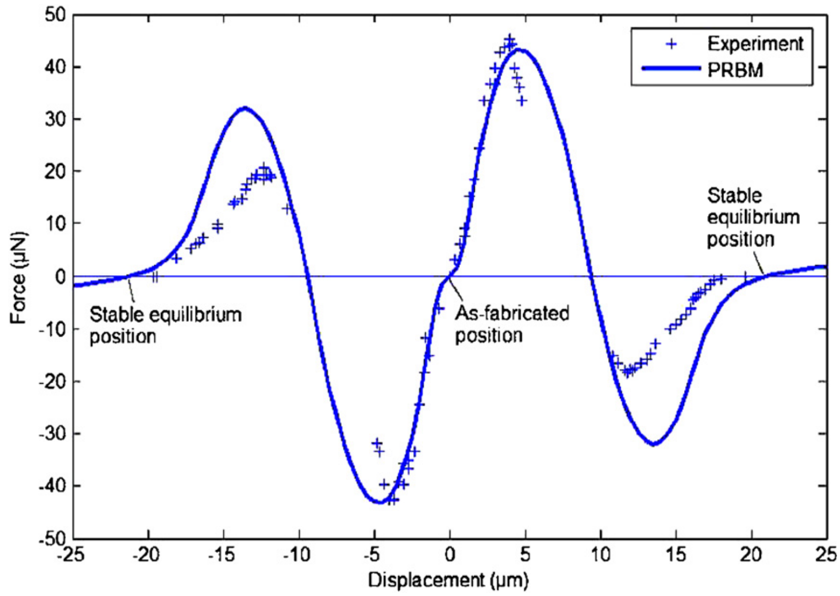

Figure 7. Results comparison of the experiment and the PRBM.

$$r_4 = \sqrt{l_{m1}^2 + (l_{n1} + r_9)^2} \tag{31}$$

$$r_8 = \sqrt{l_{m2}^2 + (l_{n2} - r_9)^2} \tag{32}$$

$$\theta_3 = \arctan \frac{r_1 \sin\theta_1 + l_{n1} + r_9 - r_2 \sin\theta_2}{r_1 \cos\theta_1 + l_{m1} - r_2 \cos\theta_2} \tag{33}$$

$$r_3 = \frac{r_1 \cos\theta_1 + l_{m1} - r_2 \cos\theta_2}{\cos\theta_3}. \tag{34}$$

$$\theta_7 = 2\pi - \arctan \frac{-r_5 \sin\theta_5 + l_{n2} - r_9 + r_6 \sin\theta_6}{r_5 \cos\theta_5 + l_{m2} - r_6 \cos\theta_6} \tag{35}$$

$$r_7 = \frac{r_5 \cos\theta_5 + l_{m2} - r_6 \cos\theta_6}{\cos\theta_7}. \tag{36}$$

By selecting θ_1, θ_2 and F_A as the three independent variables for the upper part (equation (27)), and θ_5, θ_6 and F_B as the three independent variables for the lower part (equation (28)), this system of virtual work and kinematic equations can be solved numerically to obtain the force–deflection behavior of the tristable mechanism.

4. Test device

A DTTM was designed and fabricated to demonstrate that tristable behavior is achievable, to show that the ideas discussed above are applicable for micromechanisms, and to provide a test device with which to gather experimental data for comparison to the model.

DTTMs were designed in polysilicon for fabricating in the SUMMiT V process (Sandia National Laboratories). The following geometric parameters were used in the device design: $L_c = 247$ μm, $w_c = 1.2$ μm, $h_c = 4.65$ μm (Poly3 and Poly4), $\theta_{1o} = 3.87°$, $L_s = 19.3$ μm, $w_s = 1$ μm, $h_s = 4.5$ μm, $\theta_{2o} = 2.75°$, $L_m = 30$ μm and $L_n = 6.3$ μm. The predicted force–deflection behavior using the PRBM is shown in figure 7. To facilitate data gathering for comparison to model predictions, a force gauge [23] and a vernier were included, as shown in figure 8. This set-up allows for measurement of force–displacement measurements through much of the motion. This is done by optically measuring the displacement at the vernier, and determining the required force to cause that displacement in the force gauge for its known design and stiffness.

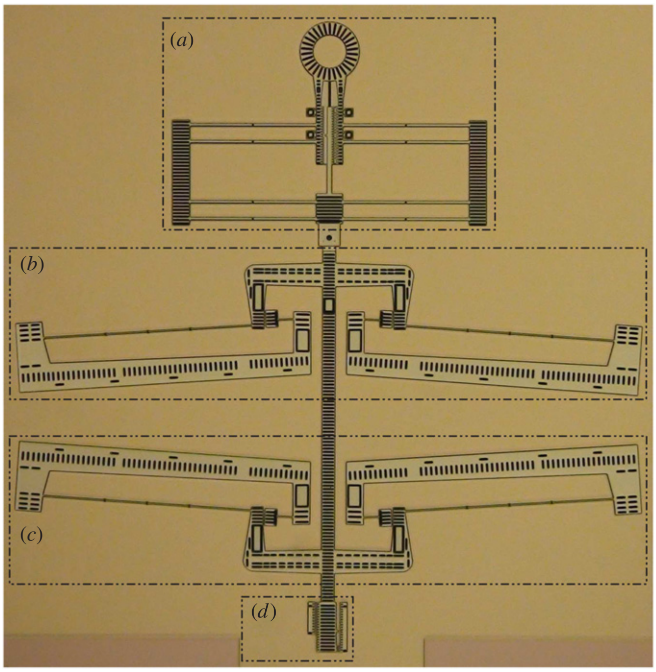

Figure 8. Fabricated position (first stable equilibrium position). (*a*) Force gauge, (*b*) upper part, (*c*) lower part and (*d*) vernier.

Due to an in-plane over-etch (0.1 μm per side) that is inherent to SUMMiT V, the thickness of a fabricated beam is less than its designed value. Because the mechanism's

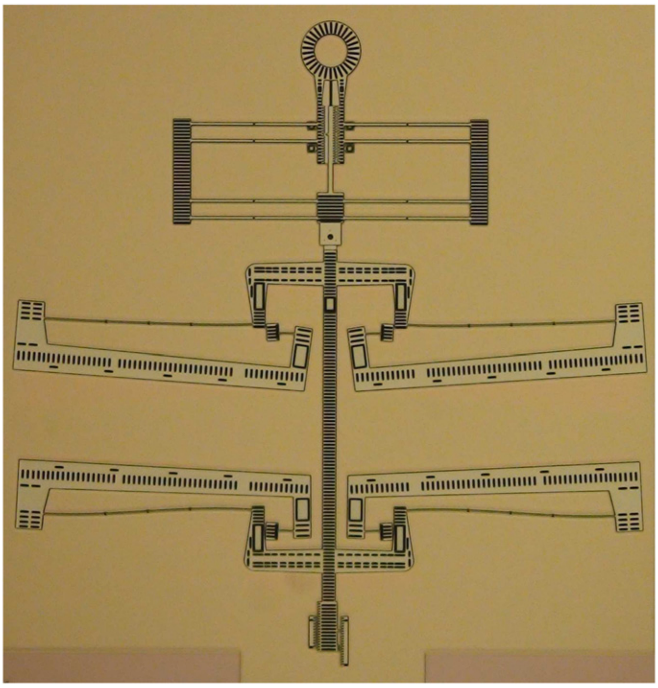

Figure 9. The second stable equilibrium position. Note the deflection in the lower part. The device has moved up relative to its undeflected position.

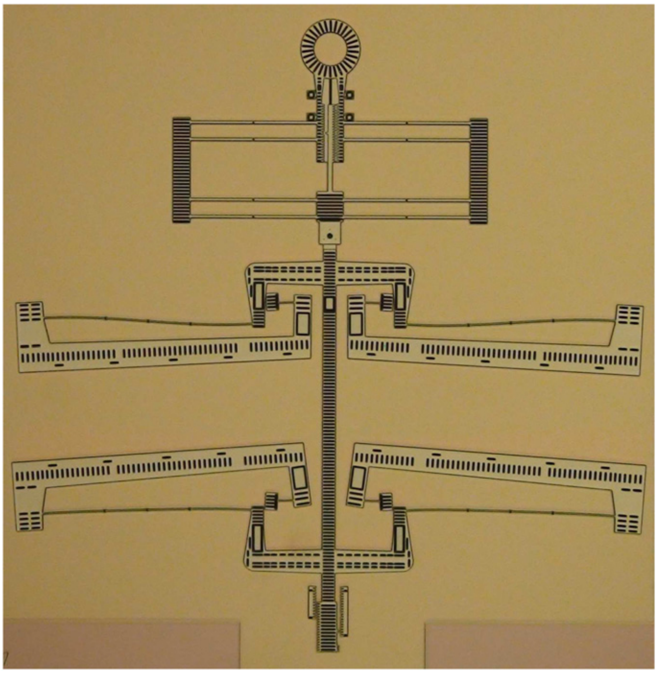

Figure 10. The third stable equilibrium position. Note the deflection in the upper part. The device has moved down relative to its undeflected position.

deflection is in-plane, this can have a large effect on the measured results [13]. The design parameters were adjusted to account for the as-fabricated geometry.

A scanning electron micrograph of a DTTM, without force gauge, is shown in figure 2. Figure 8 is an optical image of the DTTM and shows its upper and lower parts. The force gauge and vernier are also shown and labeled on the figure.

5. Results

5.1. Tristable behavior

Testing successfully demonstrated consistent tristable behavior for multiple devices. A microprobe was used to move the devices between stable equilibrium positions. The measured force–deflection behavior is shown in figure 7. Figure 8 shows the first stable equilibrium or as-fabricated position. The second stable equilibrium position is shown in figure 9. The upper and lower flexible beams have different deflected shapes in this position, as predicted. The upper part acts as a bistable mechanism and the lower part as a soft spring. Figure 10 shows the third stable equilibrium position. Now the lower part provides the bistable behavior while the upper part is a soft spring. The second and third positions are symmetric about the first positions, as expected.

The model successfully predicted the tristable behavior and made a reasonable prediction for the location of the stable equilibrium positions. The predicted and measured values for the stable equilibrium positions are listed in table 4. The difference between the modeled and predicted values is attributed to the effects of friction on the measurement devices (force gauge and vernier) that are suspended from the DTTM

Table 4. The predicted and measured values for the stable equilibrium positions.

	Predicted	Measured
First stable position (μm)	0	0
Second stable position (μm)	21.1	19.6
Third stable position (μm)	−21.1	−19.7

(the friction between the moving parts and the substrate). Friction would cause the device to come to equilibrium at a position sooner than predicted for the ideal case.

5.2. Force–displacement behavior

The force–displacement behavior of the DTTM is shown in figure 7. The predicted values for the maximum force from the first stable equilibrium position to the second and third stable equilibrium positions match the experimental results well. The small difference can be attributed to the friction effects caused by the suspended measurement devices. This is consistent with the measured force, which includes friction resisting the motion, being larger than the predicted force. It is also consistent with the differences in equilibrium positions. The force measured returning from the second or third to the first stable equilibrium position was lower than predicted, as shown in figure 7. This difference is likely due to the DTTM undergoing some out-of-plane motion during that segment of travel. This would be consistent with the behavior recently found for some bistable micromechanisms [24]. That research found that some eccentric loads could cause unanticipated out-of-plane motion that may result in lower than predicted forces.

This motion can be eliminated by constraining out-of-plane motion with stops or higher aspect ratio flexures. However, this part of the force deflection path is noncritical for many applications and the lower than expected force may actually be a benefit in some cases.

6. Conclusion

A fully compliant tristable mechanism, in which the flexible segments undergo tension, compression and bending, is introduced as the fully compliant double tensural tristable mechanism (DTTM). A DTTM has been demonstrated to have the following characteristics:

- The mechanism provides three stable positions.
- The output displacement of the mechanism is linear and parallel to the mechanism's shuttle.
- The mechanism is fully compliant (i.e., it does not require any sliding or rotating joints).
- Tensural pivots are used in the mechanism to achieve tristability.

Potential applications of the DTTM include three-way switches (single-pole-double throw switches), multiplex optical switches and mechanical memory.

A pseudo-rigid-body model (PRBM) for the DTTM has been developed. Although the model is a six degree-of-freedom model, the mechanism position can be predicted with only one input by finding the lowest energy state for that position. The PRBM can be used to identify tristable configurations and predict the performance of the DTTMs. It may be particularly useful to design DTTMs with customized behavior. The model predicted well the performance of the DTTM and DTTMs were demonstrated to have tristable behavior.

Acknowledgments

The authors gratefully acknowledge the financial support from the National Natural Science Foundation of China under Grant No. 50805110 and the China Postdoctoral Science Foundation under Grant No. 20070421110.

References

[1] Howell L L 2001 *Compliant Mechanisms* (New York: Wiley)
[2] Jensen B D and Howell L L 2003 Identification of compliant pseudo-rigid-body mechanism configurations resulting in bistable behavior *Trans. ASME, J. Mech. Des.* **125** 701–8
[3] Jensen B D and Howell L L 2004 Bistable configurations of compliant mechanisms modeled using four links and translational joints *Trans. ASME, J. Mech. Des.* **126** 657–66
[4] Su H and McCarthy J M 2007 Synthesis of bistable compliant four-bar mechanisms using polynomial homotopy *Trans. ASME, J. Mech. Des.* **129** 1094–8
[5] Wilcox D L and Howell L L 2005 Fully compliant tensural bistable micromechanisms (FTBM) *J. Microelectromech. Syst.* **14** 1223–35
[6] Qiu J, Lang J H and Slocum A H 2004 A curved-beam bistable mechanism *J. Microelectromech. Syst.* **13** 137–46
[7] Hälg B 1990 On a micro-electro-mechanical nonvolatile memory cell *IEEE Trans. Electron Devices* **37** 2230–36
[8] Charlot B, Sun W, Yamashita K, Fujita H and Toshiyoshi H 2008 Bistable nanowire for micromechanical memory *J. Micromech. Microeng.* **18** 1–7
[9] Foulds I G, Trinh M T, Hu S, Liao S W, Johnstone R W and Parameswaran M A 2003 New design for surface micromachined bistable and multistable switches *J. Microlith., Microfab., Microsyst.* **2** 255–8
[10] Hwang I, Shim Y and Lee J 2003 Modeling and experimental characterization of the chevron-type bi-stable microactuator *J. Micromech. Microeng.* **13** 948–54
[11] Kwon H N, Hwang I and Lee J 2005 A pulse-operating electrostatic microactuator for bi-stable latching *J. Micromech. Microeng.* **15** 1511–6
[12] Masters N D and Howell L L 2003 A self-retracting fully compliant bistable micromechanism *J. Microelectromech. Syst.* **12** 273–80
[13] Wilcox D L and Howell L L 2005 Double-tensural bistable mechanisms (DTBM) with on-chip actuation and spring-like post-bistable behavior *Proc. 2005 ASME Mechanisms and Robotics Conference: DETC2005-84697*
[14] Oberhammer J, Tang M, Liu A Q and Stemme G 2006 Mechanically tri-stable, true single-pole-double-throw (SPDT) switches *J. Micromech. Microeng.* **16** 2251–8
[15] Pendleton T M and Jensen B D 2007 Development of a tristable compliant mechanism *Proc. 12TH IFToMM World Congress* A835
[16] Han J S, Muller C, Wallrabe U and Korvink J G 2007 Design, simulation, and fabrication of a quadstable monolithic mechanism with X- and Y-directional bistable curved beams *Trans. ASME, J. Mech. Des.* **129** 1198–203
[17] Ohsaki M and Nishiwaki S 2005 Shape design of pin-jointed multistable compliant mechanisms using snapthrough behavior *Struct. Multidisc. Optim.* **30** 327–34
[18] Oh Y S and Kota S Synthesis of multi-stable equilibrium compliant mechanisms using combinations of bistable mechanisms *Trans. ASME, J. Mech. Des.* at press
[19] King C W, Beaman J J, Sreenivasan S V and Campbell M 2004 Multistable equilibrium system design methodology and demonstration *Trans. ASME, J. Mech. Des.* **126** 1036–46
[20] King C W, Campbell M, Beaman J J and Sreenivasan S V 2005 Synthesis of multistable equilibrium linkage systems using and optimization approach *Struct. Multidisc. Optim.* **29** 477–87
[21] Howell L L and Midha A 1996 A loop-closure theory for the analysis and synthesis of compliant mechanisms *Trans. ASME, J. Mech. Des.* **118** 121–5
[22] Masters N D and Howell L L 2005 A three degree-of-freedom model for self-retracting fully compliant bistable micromechanisms *Trans. ASME, J. Mech. Des.* **127** 739–44
[23] Wittwer J W, Gomm T and Howell L L 2002 Surface micromachined force gauges: uncertainty and reliability *J. Micromech. Microeng.* **12** 13–20
[24] Cherry B B, Howell L L and Jensen B D 2008 Evaluating three-dimensional effects on the behavior of compliant bistable micromechanisms *J. Micromech. Microeng.* **18** 095011